22

The Plasmasphere: Its Interactions and Dynamics

Fabien Darrouzet,[1] Dennis L. Gallagher[2], and Johan De Keyser[1]

ABSTRACT

This chapter is a review of plasmaspheric research accomplishments published from September 2013 to September 2018. Much has been achieved during these five years, most of which we hope to have cited in the references section. Research has addressed plasmasphere interactions with the ionosphere and thermosphere, but also with the energetic particles of the ring current and radiation belts. Internal physical processes that shape plasmaspheric properties have been studied, as well as those that result from external driving by the solar wind through the geomagnetic response. New empirical and physics-based models of the plasmasphere have been introduced to the field as well. Conclusions about these five years of plasmaspheric research are provided, in addition to our view of the future investigations.

22.1. INTRODUCTION

The plasmasphere is the upward extension of the Earth's ionosphere at low to middle geomagnetic latitudes. It is a torus-like region of dense and cool plasma of ionospheric origin (density between 10 and $10^4\,cm^{-3}$ and energy of a few eV) trapped on closed geomagnetic field lines (see books by Lemaire and Gringauz, 1998; Darrouzet et al., 2009, and references therein). The plasmasphere's configuration, size, shape and plasma distribution depend sensitively on the recent geomagnetic activity.

22.1.1. Plasmasphere Processes and Magnetosphere Global System

The plasmasphere is mainly driven by the magnetospheric electric field at high altitude, and by the forcing from the ionospheric electric field at low altitude. After the arrival of a solar wind disturbance at Earth or during a magnetospheric substorm, the dawn–dusk electric field becomes stronger, which alters the magnetospheric convection. This subsequently erodes away the outer regions of the plasmasphere. As a result, the plasmasphere develops a sharp outer boundary, the plasmapause. If the disturbance is strong enough (a minimum Dst index of −30 nT and/or a minimum *Kp* index of 3 during the previous 24 hours would be sufficient), a plume can be formed and other density structures may be created as well. The evolution of eroding plasma depends on the magnetospheric electric field and how it develops over time. It is, for example, not impossible that eroding plasma from an initially forming plume stops convecting further outwards, thus forming a plasmasphere shoulder. One can also imagine that the plume plasma is convected back inwards towards the bulk of the plasmasphere. But normally the eroding material is lost as a plume that moves outward, so that the plasma is effectively removed through the magnetospheric boundary or through the tail.

As the magnetospheric electric field recovers, the plasmasphere is refilled from the ionosphere on a time scale of hours to days. The ionospheric convection pattern

[1]*Royal Belgian Institute for Space Aeronomy, Brussels, Belgium*

[2]*NASA Marshall Space Flight Center, Huntsville, AL, USA*

Space Physics and Aeronomy Collection Volume 2: Magnetospheres in the Solar System, Geophysical Monograph 259, First Edition.
Edited by Romain Maggiolo, Nicolas André, Hiroshi Hasegawa, and Daniel T. Welling.

DOI: 10.1002/9781119815624.ch22

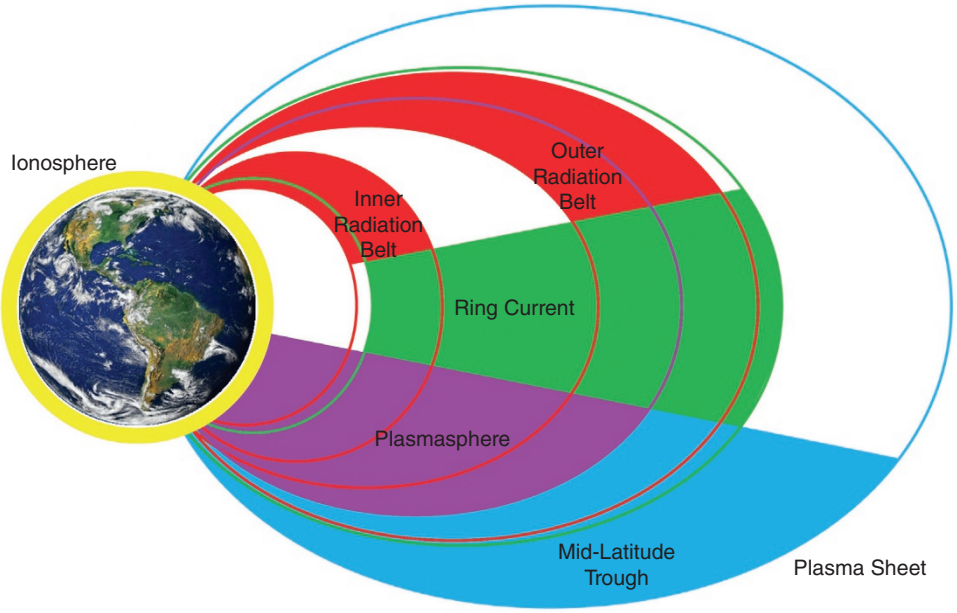

Figure 22.1 Sketch of the inner magnetosphere, describing the regions discussed in this chapter: the ionosphere in yellow, the plasmasphere in purple, the inner and outer radiation belts in red, the ring current in green, and the mid-latitude trough in blue.

(controlled by the ionospheric electric potential and by the neutral atmosphere through ion-neutral friction) at the same time affects the plasmaspheric flow. The plasmasphere is also connected to the ring current and the radiation belts (Figure 22.1). Thus the plasmasphere is part of the global magnetospheric system described in this review book. This governs the structure of this chapter, as detailed in the outline (section 22.1.4). Before reviewing recent progress in plasmasphere science, we discuss the few reviews that were published (section 22.1.2), and the new tools and techniques developed to study the plasmasphere and to better understand its complexity (section 22.1.3).

22.1.2. Previous/Recent Plasmasphere Reviews

A few review papers about the plasmasphere have been published since 2013. Darrouzet and De Keyser (2013) reviewed some results of studies published between 2009 and 2012 about the global evolution of the plasmasphere under the increase of geomagnetic activity. Green (2015) summarized the results obtained with the IMAGE (Imager for Magnetopause-to-Aurora Global Exploration) spacecraft, ten years after its loss in December 2005. A ground-based perspective has been offered by Menk et al. (2014). A special section on inner magnetosphere coupling appeared in the *Journal of Geophysical Research* (Usanova and Shprits, 2017). A review of the various manifestations of plasmaspheric plumes in different types of measurements in different regions by Moldwin et al. (2016) emphasizes the strong two-way coupling between the magnetosphere and the ionosphere when geomagnetic activity is high. A book chapter about EMIC waves in the inner magnetosphere has been compiled by Usanova et al. (2016).

22.1.3. New Tools/Techniques

Direct measurement of the temperature of the low energy electrons in the Earth's plasmasphere is difficult. For that reason Boardsen et al. (2014) developed a new method to compute this quantity by solving current balance equations for the electric field probes and the body of the Polar spacecraft. For the ion temperature, Genestreti et al. (2017) developed two techniques using an electrostatic analyzer-based instrument onboard Van Allen Probes. The first technique applies a constrained theoretical fit to a measured distribution function. The second technique involves the comparison of total and partial energy number densities. Exploiting the effect of the Earth's optical shadow on thermal plasma measurements made by the Interball satellites in the plasmasphere, Kotova et al. (2014) determined the spacecraft potential and the plasma density and temperature. Hartley et al. (2018) presented a new method to infer electron density in the plasmasphere from the electric and magnetic wave power associated with plasmaspheric hiss, relying on the cold plasma dispersion relation.

To improve analysis of images from the EUV (Extreme UltraViolet) instrument onboard the IMAGE satellite, Goldstein et al. (2017) proposed a new empirical technique to determine the background levels of 30.4 nm extreme ultraviolet emission. Nakano et al. (2014) developed a new method to estimate the temporal evolution of the plasmaspheric helium ion density: by combining several IMAGE/EUV images they obtained the helium density profile along a field line. By defining the plasmapause as the radial distance with the sharpest negative radial He^+ density gradient at each MLT (magnetic local time) within each usable EUV image, Katus et al. (2015) developed a new automatic tool to derive the plasmapause position.

Yan et al. (2016) improved the quality of the meridian-view plasmasphere images taken by the Moon-based Extreme Ultraviolet Camera (EUVC) onboard Chang'e-3 through a proper denoising of the images and a more accurate geometric positioning. He et al. (2016) developed an automatic detection of the plasmapause location in those images using a minimum L algorithm.

Field-aligned ducts are present in the plasmasphere and they guide whistler waves along magnetic field lines. A new technique for detecting those ducts has been developed using a novel ground-based radio telescope array imaging technique (Loi et al., 2015).

22.1.4. Outline of the Chapter

The plasmasphere is part of a highly coupled system. It interacts with the ionosphere and thermosphere as described in section 22.2, and with ring current and radiation belts particles as presented in section 22.4. The plasmaspheric response to solar wind driving and geomagnetic acticity is developed in section 22.3. The state of plasmaspheric modeling is presented in section 22.5 and future opportunities for plasmasphere research are outlined in the last section 22.6. Rather than presenting an exhaustive/complete review of all plasmasphere research, the goal of this overview is to focus on key aspects of plasmaspheric interactions and dynamics.

22.2. PLASMASPHERE INTERACTIONS WITH THE IONOSPHERE AND THERMOSPHERE

The plasmasphere interacts with the ionosphere and the thermosphere through several physical processes. Some recent work about these coupling processes is presented below. Note that the global magnetosphere–ionosphere coupling is presented in Part IV of this book.

22.2.1. Cold Ion Distribution

The distribution of cold plasma along a plasmaspheric magnetic flux tube is usually considered to be nearly constant within 30–40° of the magnetic equator, and rapidly increasing as the ionosphere is approached. A recent study of Interball data has shown the dependence of the H^+ ion concentration also on geographic longitude (Chugunin et al., 2017): During summer in the near-midnight sector and for a constant McIlwain parameter $L = 2.5$, the minimum in the H^+ concentration falls within geographic longitudes of 270°–315°. This corresponds to the east North American sector in the Northern Hemisphere and to the Antarctic Peninsula in the Southern Hemisphere.

The plasma density in the plasmasphere boundary layer (PBL) has been studied with MAGION 5 data by Kotova et al. (2018). The authors found it to be inversely proportional to the volume of the unit magnetic flux tube. The PBL width appears to depend linearly on the time elapsed since the most recent maximum value of the *Kp* index.

Knowledge of the field-aligned ion distribution is important to understand better the plasmasphere refilling process. It can also serve as a priori information facilitating the inversion of EUV images of the plasmasphere into densities. Using IMAGE data, Reddy et al. (2018) determined the evolution of the field-aligned H^+, He^+ and O^+ densities from $L = 2$–3 on the dayside during a geomagnetically quiet to moderately active period. They derived an O^+/H^+ transition height (altitude where both number densities are equal) of 880 ± 60 km and 1000 ± 100 km at $L \sim 2$ and $L \sim 3$, respectively (Figure 22.2).

22.2.2. Refilling – Outflow

Following a storm or substorm, the outer plasmasphere is eroded and after a while it is refilled from the ionosphere. This phenomenon is not yet fully understood (for a review of unsolved problems in plasmasphere refilling, see Gallagher and Comfort, 2016), but some progress has been made during the last years.

André et al. (2015) determined with Cluster data a global ionospheric outflow of the order of 10^{26} ions s^{-1}, and up to twice that much with increasing solar EUV flux at solar maximum. The occurrence rates of both plumes and outflow events at the dayside magnetopause increase with solar wind dynamic pressure (Lee et al., 2016).

The influence of the thermosphere on the refilling rates has been studied with different models by Krall et al. (2016). They showed that modest decreases in thermospheric density and exospheric temperature can lead to large increases in plasmaspheric refilling rates and that changes in the thermospheric wind pattern can have a similar effect. Denton and Borovsky (2014) found that the neutral atmosphere number density is critical in controlling the rate of refilling at geosynchronous orbit. In a study of refilling of the plasmasphere during extended quiet periods with Cluster data by Lointier et al. (2013),

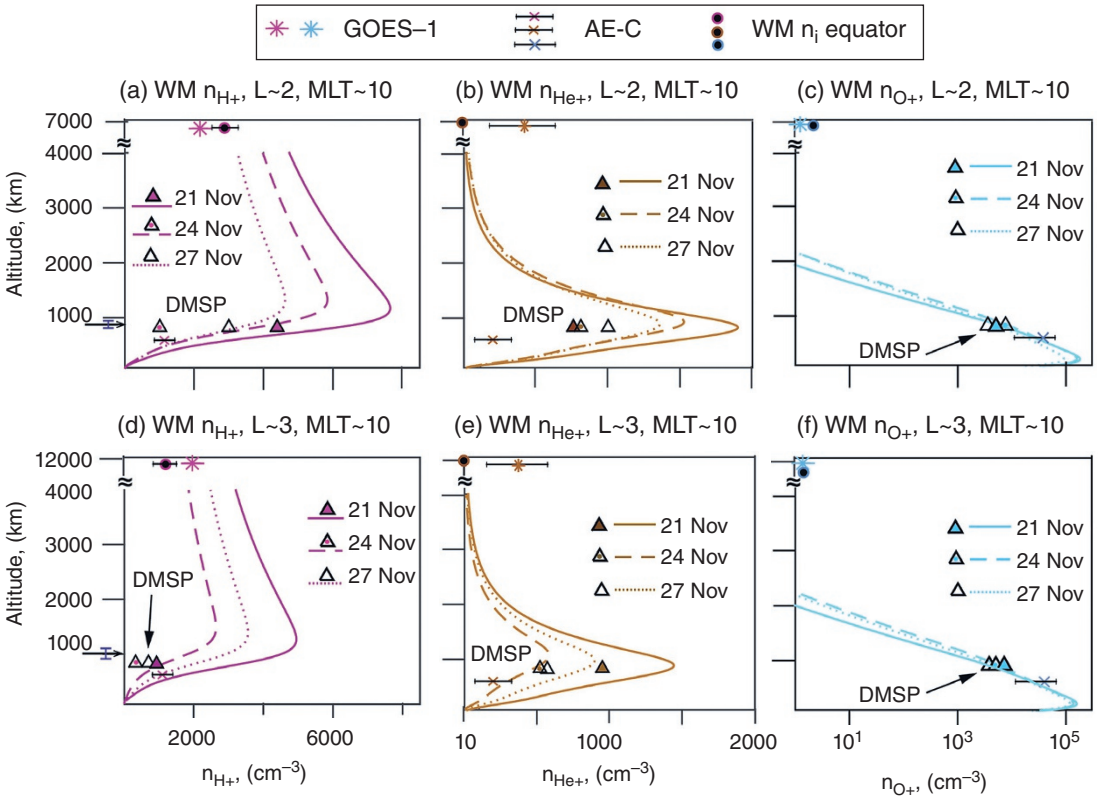

Figure 22.2 Evolution of field-aligned H^+ (pink), He^+ (brown), and O^+ (cyan) densities at (a–c) $L \sim 2$ and (d–f) $L \sim 3$ during the 21–27 November 2005 period as obtained from whistler mode radio sounding. The color-coded black-filled circles represent whistler-mode sounding measurements of ion densities extrapolated to equatorial altitudes. Also shown are past measurements of equatorial ion densities by GOES (Geostationary Operational Environmental Satellite)-1 (color-coded stars), near-simultaneous in situ measurements from the DMSP (Defense Meteorological Satellite Program)-F15 spacecraft (color-coded triangles), and past measurements of ion densities by the AE (Atmospheric Explorer)-C satellite (color-coded crosses). The arrows on the altitude axis in panels (a) and (d) represent the O^+/H^+ transition height obtained from whistler mode sounding measurements of ion densities. (Adapted from Reddy et al., 2018.)

it was found that magnetic flux tubes are not fully replenished even after six days of quiet conditions. Also, there appears to be an MLT dependence in the refilling rate.

22.2.3. Ionosphere Coupling

The ionospheric mid-latitude trough is a depleted region of ionospheric plasma density in the nightside F region and lies just equatorward of the auroral region. Chen et al. (2018) highlighted the differences between the plasmapause and this mid-latitude trough with data from the DEMETER (Detection of Electro-Magnetic Emissions Transmitted from Earthquake Regions) mission. The trough usually appears on the poleward side of the plasmapause, which is sensitive to solar activity, while the trough has a stronger response to seasonal variation.

Using total electron content (TEC) measurements, Lee et al. (2013) investigated the global morphology of the plasmasphere density in relation to the ionosphere. The plasmasphere exhibits much weaker diurnal variations, and while the annual ionospheric variability exists regardless of longitude, it occurs only in the American sector for the plasmasphere. Shim et al. (2017) used the Jason 1 satellite to build a climatology of the plasmaspheric TEC (pTEC) between 1,336 km and 20,200 km. Their conclusion is that pTEC variability is significantly different from that of TEC.

The equatorward boundary of small-scale field-aligned currents and its relation with the plasmapause have been investigated by Heilig and Lühr (2018). The authors found that both boundaries respond similarly to changes in geomagnetic activity and that they are closely located in the near midnight MLT sector, suggesting a dynamic linkage.

Other details about the interaction between the plasmasphere and the ionosphere are presented in this book in Chapter 23.

22.2.4. The Outer Plasmasphere

The plasmapause erosion and the equatorward expansion of the auroral oval after substorm onset occur almost simultaneously in both MLT and UT (universal time) sectors, as shown with Chang'e-3 data (Zhang et al., 2017). There is a clear causal link driving both phenomena: the changing magnetospheric electric field and the corresponding convection pattern.

As part of the changing global electric field during a substorm, the plasma trough and plasmasphere boundary region between the auroral zone and the plasmasphere proper also undergo changes. The subauroral polarization stream (SAPS) is a strong, latitudinally narrow subauroral velocity field observed in the evening and early morning local time sector. The SAPS is an important magnetosphere–ionosphere coupling signature. With MMS (Magnetospheric MultiScale) data and ground-based radar observations, Erickson et al. (2016) observed typical localized SAPS electric fields in the plasmasphere boundary region. These features most likely reflect SAPS ionospheric structure, which demonstrates the ionosphere's importance in regulating fine-scale magnetosphere–ionosphere coupling.

During the recovery phase of a magnetic storm, proton aurora spots may appear. Their projection onto the equatorial plane has been compared with the (modeled) plasmapause position. Most of the events map within 0.5 R_E from the plasmapause (Yahnin et al., 2013).

22.3. PLASMASPHERIC RESPONSE TO SOLAR WIND DRIVING AND GEOMAGNETIC ACTIVITY

The general circulation in the plasmasphere is a consequence of the solar wind–magnetosphere interaction. Variations in the solar wind driver directly affect the plasmaspheric response. Some recent studies on this topic are described in this section.

22.3.1. Erosion

After an increase of solar activity leading to a storm or a substorm, the plasmasphere is eroded. This erosion has been studied with the coupled ionosphere–inner magnetosphere model SAMI3/RCM (Sami3 is also A Model of the Ionosphere/Rice Convection Model) (Krall et al., 2017). The model predicts a strong erosion outside of a sharp, poststorm plasmapause and a weak erosion inside the plasmapause.

The plasmasphere erosion flux can be derived from in situ observations. In an event study, Foster et al. (2014) found a value of $1.2 \times 10^{12}\,\mathrm{m^{-2}\,s^{-1}}$ with similar low- and high-altitude characteristics. Using Van Allen Probes data, Sarno-Smith et al. (2015) showed that H^+ is depleted the most in the postmidnight sector (1–4 MLT), followed by O^+ and then He^+, due to diurnal ionospheric temperature variation and charge exchange processes (Figure 22.3).

Another phenomenon is responsible for plasma escaping from the plasmasphere: the plasmaspheric wind, which steadily transports cold plasmaspheric plasma outwards across the geomagnetic field lines, even during prolonged periods of quiet geomagnetic conditions. It has been experimentally detected using the Cluster satellites by Dandouras (2013).

22.3.2. Solar Wind Transients

The plasmapause location is directly influenced by solar wind variations. Using Cluster data, Verbanac et al. (2015) studied the relationships between the plasmapause position and several solar wind coupling parameters and functions. They showed that to describe the plasmapause response to any disturbances, it is more appropriate to choose the value of those parameters/functions at the highest correlation time lag rather than the maximum value prior to the plasmapause crossing. The coupling function giving the best indicator in all MLT sectors is the product of the magnitude of the interplanetary magnetic field and the solar wind velocity, which is related to the strength of the interplanetary electric field (IEF).

Katus et al. (2015) analyzed IMAGE data to determine the plasmapause location. They showed that for magnetic cloud-driven events, and early in the main phase, the plasmapause is closer to the Earth while for sheath-driven storms it remains farther from the Earth at the start of the main phase but moves further earthward during continued convection approaching the storm peak.

22.3.3. Geomagnetic Activity

It is of course also valuable to study the plasmasphere and plasmapause across the full range of geomagnetic conditions from quiet to active. For example, Kwon et al. (2015) examined the plasmapause location under quiet geomagnetic conditions ($Kp \leq 1$) using the electron density inferred from the spacecraft potential determined by the THEMIS (Time History of Events and Macroscale Interactions during Substorms) satellites. During those quiet geomagnetic activity periods, a slight plasmaspheric bulge is observed in the dusk sector and the plasmapause extends nearly up to geosynchronous orbit in all MLT sectors. Those results confirm the general model for the plasmapause profile being driven globally by a combination of the magnetospheric convection and corotational electric fields. They are also in agreement with previous geosynchronous observations.

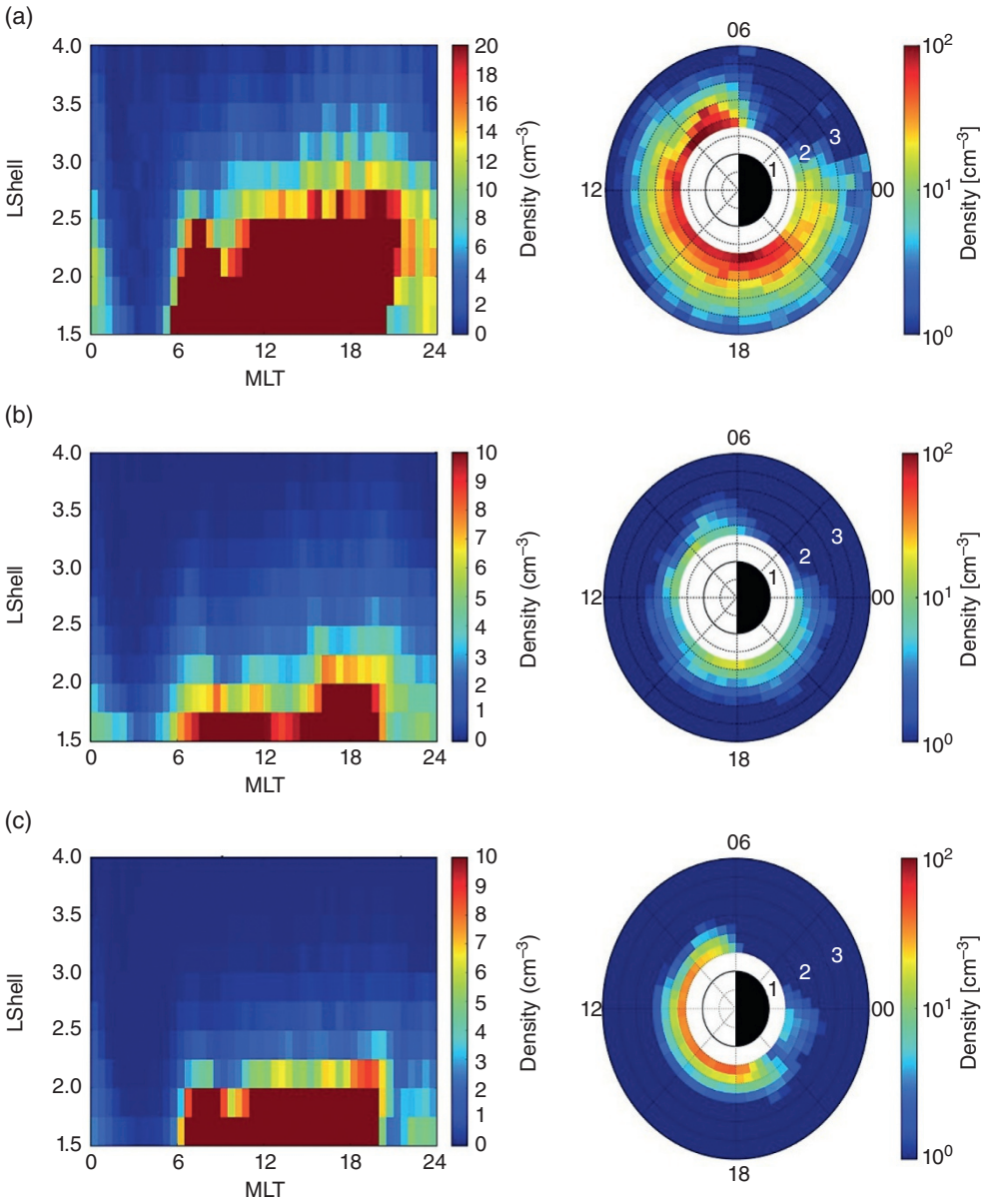

Figure 22.3 Median partial plasma density from 1 to 4 eV measured by HOPE during quiet times over a 22-month period for (a) H^+, (b) He^+, and (c) O^+. The density maps on the right are on a logarithmic scale, while the maps on the left are on a relative linear scale dependent on species. (Adapted from Sarno-Smith et al., 2015.)

The plasmapause shape for different levels of geomagnetic activity and the delays in the MLT response of the plasmapause have been computed with CRRES (Combined Release and Radiation Effects Satellite) data by Bandić et al. (2016). They found that the plasmaspheric bulge is formed in the postdusk at high geomagnetic activity and close to midnight at low geomagnetic activity.

The plasmaspheric mass density can be derived from (space- and ground-based) field line resonance (FLR) observations. This information is important because space-based measurements often lack compositional information, while it is known that the plasmasphere contains contributions not only from H^+ but also from heavy ions. Few results have been published on this important topic. Using LANL (Los Alamos National Laboratory) and IMAGE satellites, Denton et al. (2014) demonstrated that variations in the geomagnetic activity greatly affect electron density across plumes and their adjacent regions but remarkably not mass density. From a statistical analysis of the plasmaspheric mass density as a function of

local time, Chi et al. (2013) identified an increase in mass density in the afternoon hours at all the latitudes studied, and a further density increase in the evening hours for L values between 2 and 3.

22.3.4. Plumes at the Magnetopause – Reconnection

During geomagnetic storms an enhanced global convection electric field often draws outer plasmaspheric plasma into a plume that can reach all the way to a dayside magnetopause reconnection site. A statistical study with THEMIS data has shown the presence of plume plasma at the dayside magnetopause during 12.5 % of the crossings (Walsh et al., 2013). The presence of dense and cold plasma near the dayside reconnection region suggests the possibility that it could mass-load the plasma and thus influence the reconnection process. Indeed, Walsh et al. (2014) analyzed three events that exhibit bursty and patchy reconnection jets coincident with a plume.

Toledo-Redondo et al. (2016) analyzed Cluster observations of cold ions at the dayside magnetopause during magnetic reconnection events in which those ions are heated by waves and by large electric field gradients inside the separatrix region close to the X-line. Zhang et al. (2018a) used THEMIS data to detect cold ions of plasmaspheric plume origin near the subsolar magnetopause. Those particles may have been separately accelerated by the rotational discontinuity and the slow shock inside the reconnection layer. Based on simulations, Ouellette et al. (2016) and Wang et al. (2016) found that the local and total dayside reconnection rates are reduced when a plasmaspheric plume is observed on the dayside magnetopause.

Looking for magnetospheric cold ions on the dusk flank of the magnetopause with MMS data, Fuselier et al. (2016) detected only ions from the ring current and the warm plasma cloak, but not from plasmaspheric plume due to their energy being too low for the instrumentation. The observed ions have little effect on reconnection at the duskside magnetopause, mainly due to their low density contribution to the reconnection region. Only cold dense plasmaspheric plasma has the potential to provide that influence.

22.4. PLASMASPHERE INTERACTIONS WITH ENERGETIC PARTICLES

The plasmasphere interacts with the colocated energetic particles that make up the ring current and radiation belts, in particular through wave–particle interaction. Note that a chapter of the book is dedicated to wave-particle interactions in the magnetosphere (Chapter 6).

22.4.1. Wave Distribution and Propagation

Plenty of waves are observed in the plasmasphere and all have a direct influence on the plasmasphere and its surrounding regions.

For instance, ULF (ultra low frequency, 2 mHz–5 Hz) waves play a role in the dynamics of the plasmasphere. Their propagation is controlled by the high mass density inside the plasmasphere. This can cause energization and radial transport of electrons whose drift times are comparable to the ULF periods (Hudson et al., 2014). Using THEMIS data, Liu et al. (2013) showed poloidal ULF waves excited within the PBL where the eigenfrequency was close to the bounce frequency of protons. They suggested also that cold plasma density seems to be a controlling factor for ULF wave generation. Zong et al. (2017) found in Cluster data that low-energy plasmaspheric electrons could be accelerated by third harmonic mode ULF waves excited by interplanetary shocks. Ren et al. (2018) showed with Van Allen Probes observations that cold plasmaspheric electrons can be accelerated through a drift-bounce resonance with ULF waves.

Electromagnetic ion-cyclotron (EMIC) waves are transverse plasma waves generated in the inner magnetosphere by ring current ions with perpendicular temperature anisotropy. EMIC are detected in space and on the ground in the Pc1-2 frequency range (0.1–5 Hz). Based on data from CRRES, Halford et al. (2015) showed that the cold plasma density is important for EMIC waves in the radiation belts, as those waves are found in enhanced cold plasma density regions, but not necessarily inside plumes. Usanova et al. (2013) found EMIC waves only 10% of the time when Cluster crossed plumes along its polar orbit. Moreover, enhanced solar wind dynamic pressure significantly increases EMIC wave occurrence rate inside plumes. Grison et al. (2016) studied a coherent electromagnetic rising tone recorded by the four Cluster spacecraft on the nightside of the plasmasphere. This rising tone, with a wave packet fine structure, has been excited through the nonlinear wave growth process. The authors concluded that the observed rising tone was an EMIC-triggered emission propagating toward the Earth and toward the magnetic equator at a group velocity of about 200 km s^{-1}. Observations of EMIC rising tones in the vicinity of plasmaspheric plumes (Grison et al., 2018) confirmed the importance of cold plasmaspheric plasma for nonlinear wave processes at the ion scale, in agreement with the theory.

Fast magnetosonic waves (also often called equatorial noise) are electromagnetic waves primarily confined to a narrow range around the geomagnetic equator at a frequency range between the proton gyrofrequency and the lower hybrid resonance frequency (Santolík et al., 2016). Strong magnetosonic waves were observed both outside

and inside the plasmapause during a weak storm (Xiao et al., 2015). The authors showed that those waves can enter the plasmasphere with the aid of continuous proton ring distributions.

Plasmaspheric hiss is an electromagnetic wave with an incoherent frequency-time structure observed as a steady, incoherent noise band in the typical frequency range 200–2,000 Hz and generally confined to the high-density plasmasphere. Their distribution is important for understanding energy transfer to energetic particles. For that reason Malaspina et al. (2018) used Van Allen Probes data to analyze the plasmaspheric hiss wave power distribution. They found that for $L > 2.5$, plasmaspheric hiss wave power increases with plasma density, while for $L > 3$ this increase is stronger and occurs regardless of L and MLT. Unusually intense plasmaspheric hiss waves at very low frequency down to 20 Hz have been observed by the same satellites in the dayside outer plasmasphere (Li et al., 2013). The authors showed that those waves are observed in association with and amplified by dispersed substorm-injected energetic electrons. The Van Allen Probes and THEMIS satellites have observed large-amplitude hiss waves in plasmaspheric plumes, where those waves were probably generated through instabilities involving hot electrons (Su et al., 2018). Using Cluster data, Laakso et al. (2015) showed that the plasmaspheric hiss emissions are generated in the equatorial region of the plasmaspheric plumes and that they propagate along the magnetic field lines, away from the equator. Meredith et al. (2018) compiled a new statistical model of plasmaspheric hiss including data from eight satellites. One of their main conclusions is that the hiss waves are most intense and spatially extended in the 200–500 Hz frequency band during active conditions (Figure 22.4).

Chorus waves are, like plasmaspheric hiss, right-hand polarized whistler mode electromagnetic waves propagating through the Earth's magnetosphere over a broad frequency range, from hundreds of Hz up to about 10 kHz. They are usually observed in the low-density plasma trough and mostly outside the plasmapause. However, Yu et al. (2018) detected ultra-wideband rising tone chorus waves with Van Allen Probes in a high-density region inside a plasmapause that was oscillating due to some substorm activity. The authors found that those ultra-wideband chorus waves were probably amplified through the nonlinear excitation mechanism, showing that plasmaspheric plasma is important for nonlinear wave processes.

Non-thermal continuum (NTC) terrestrial radio waves are incoherent broadband electromagnetic radiation of low intensity and long duration, observed in the frequency range from about 10 to several 100 kHz, created inside the PBL. Using Cluster data, Décréau et al. (2013) demonstrated that the source region is located in the dawn sector, at a large distance both from the Earth and from the magnetopause, at medium latitudes along the plasmapause boundary. Décréau et al. (2015) pointed out that a large portion of the PBL is radiating NTC radio waves issued from multiple sources of small size, each one radiating inside a beam of narrow cone angle.

22.4.2. Influence of Waves on Plasmasphere Electrons

Yuan et al. (2014) reported Cluster observations of plasmaspheric electron heating through Landau damping in a plasmaspheric plume. They showed that electron heating is much stronger for pitch angles of 0 and 180° than for a pitch angle of 90°. The same mechanism has been proposed to explain an energization of the thermal (<100 eV) electron population through ducted propagation of whistler waves within a plume (Woodroffe et al., 2017).

22.4.3. Influence on Ring Current Particles

Yue et al. (2018) performed a statistical survey of plasma pressure and composition of the inner magnetosphere. They found that the ring current plasma pressure is maximized inside the plasmasphere during quiet time, with ring current H^+ with energies ranging from 50 up to several 100 keV being the dominant contributor. During active times, 10–50 keV O^+ ions become important, while the He^+ contribution is generally small.

Other details about the interaction between the plasmasphere and the ring current are presented in this book in Chapter 20.

22.4.4. Influence on Radiation Belts Particles

The dynamic plasmasphere has long been recognized as a key agent in radiation belt configurations due to multiple interaction pathways between the cold plasma and more energetic particles.

The plasmasphere overlaps with the radiation belts to a varying degree. These overlap regions may be favored locations for the growth of waves that can cause loss of outer belt electrons (Summers et al., 2014). Cold dense plasmaspheric plasma may also control the propagation of ULF waves that can cause energization and radial transport of electrons (Hudson et al., 2014) but also electron precipitation (Brito et al., 2015).

Whittaker et al. (2014) conducted a superposed epoch analysis of precipitating electron observations by the POES (Polar Orbiting Environmental Satellite) constellation over 13 years in two MLT sectors. They showed that for the morning MLT sector, the precipitating electron fluxes outside the plasmapause are greatly enhanced during storm time, with this flux correlating strongly with both Dst value and distance from the plasmapause.

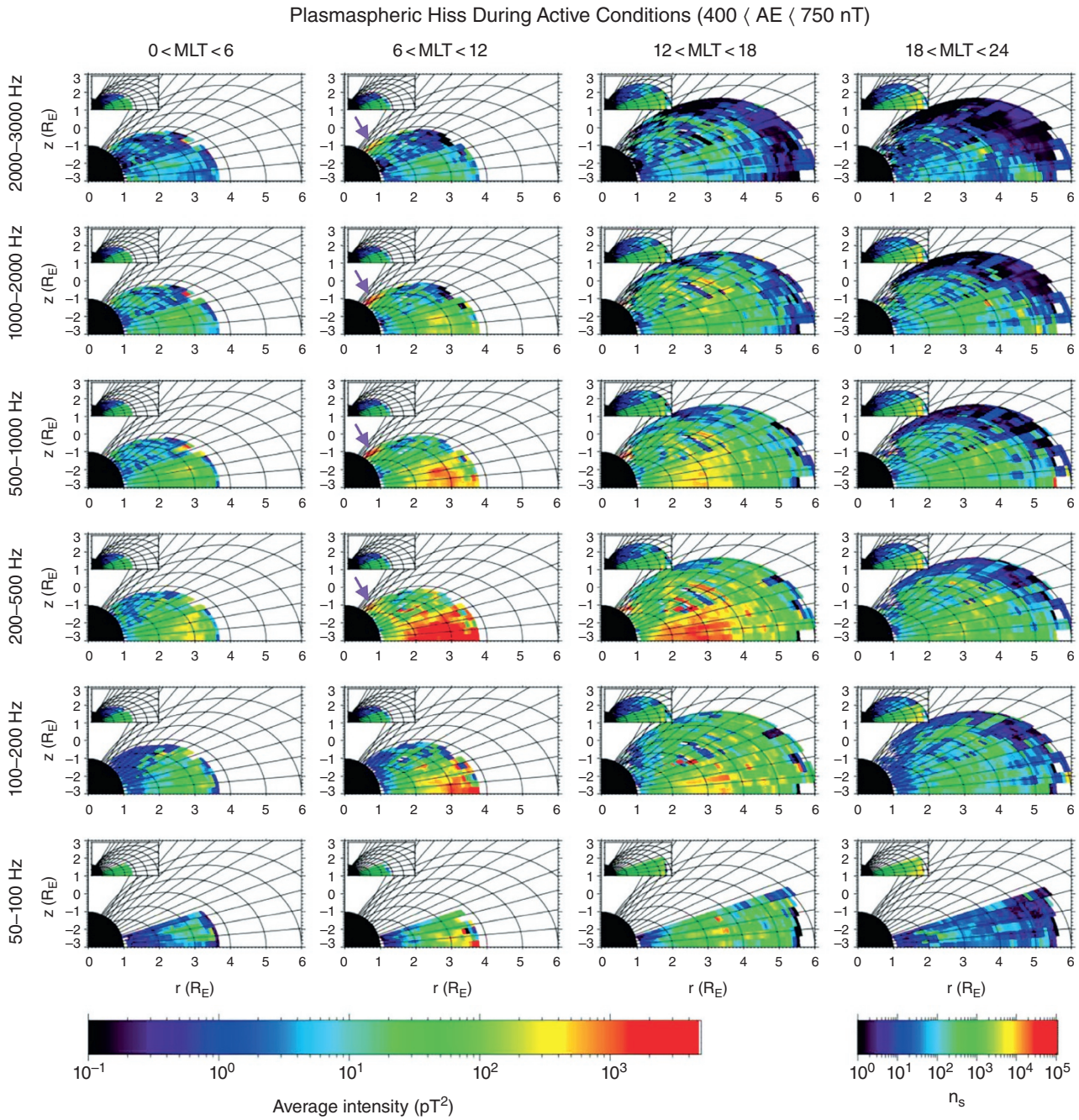

Figure 22.4 Global maps of the average wave intensity of plasmaspheric hiss in the meridional plane during active conditions, 400<AE<750 nT, for, from bottom to top, increasing wave frequency and for, from left to right, increasing MLT. To aid visualization of the data, dipole field lines and lines of constant magnetic latitude are included on the plot. The average intensities are shown in the large panels and the corresponding sampling distributions in the small panels. In the prenoon sector the purple arrows point to the location of the high-latitude plasmaspheric hiss. (Adapted from Meredith et al., 2018.)

However, the afternoon MLT sector shows time-varying precipitating electron flux inside the plasmapause dependent upon electron energy.

Goldstein et al. (2016) used Van Allen Probes data to analyze the spatial relationship between the plasmasphere and the radiation belts. They found two electron outer belts, a dynamic zone near the plasmapause and a stable zone located within 1–2 R_E inside the plasmapause. Darrouzet et al. (2013) studied the relations between the position of the plasmapause and the position of the radiation

belt boundaries with Cluster data. They showed a plasmapause position that is more variable than the radiation belt boundary positions, especially during small geomagnetic activity enhancements. During periods of low geomagnetic activity the plasmapause expands towards the outer edge of the outer radiation belt of energetic electrons (>2 MeV). At times of higher geomagnetic activity the plasmapause moves closer to the inner boundary of the outer radiation belt.

The plasmasphere may also play a role for the inner zone electrons. Indeed, Turner et al. (2015) presented an event with Van Allen Probes data revealing an injection of electrons down to $L \sim 3.5$, likely resulting from electrons interacting with a fast magnetosonic wave in the Pi2 frequency range inside the plasmasphere.

Plasmaspheric hiss waves are known to be able to pitch-angle scatter electrons in the radiation belts. In particular, hiss emissions observed inside a plasmaspheric plume are effective for pitch-angle scatter 10–100 keV electrons at rates up to $\sim 10^{-4}\,s^{-1}$ but are not able to scatter higher energy electrons (Zhang et al., 2018b). This has been confirmed by a study of plasmaspheric plume crossings at geosynchronous orbit: Borovsky et al. (2014) found a difference in the radiation belt anisotropy as a function of the plume crossing. This change is attributed to pitch-angle scattering of the radiation belt electrons during their passage through the plumes.

A statistical model of VLF (very low frequency, 3–30 kHz) waves emitted by terrestrial transmitters at $L = 1$–3 inside the plasmasphere has been provided based on Van Allen Probes data (Ma et al., 2017). The authors demonstrated a decreased lifetime for MeV electrons at low L and for keV electrons at higher L.

Other details about the interaction between the plasmasphere and the radiation belts are presented in this book in Chapter 21.

22.4.5. Influence of Meso-Scale Plasmasphere Convection on Waves

Using correlated Cluster/IMAGE observations, Adrian et al. (2015) demonstrated a direct correlation between the detection of lightning-generated whistlers beyond the plasmapause and the presence of meso-scale features created by convection at the local plasmapause, like plasmaspheric notches, crenulations, and channels. It appears that such features will facilitate the escape of those whistler waves from the plasmasphere.

22.5. THE STATE OF PLASMASPHERIC MODELING

Empirical and physics-based models are critical to advancing our knowledge of the plasmasphere. Empirical models summarize observations so they can be used to critique physical models and to reveal unknown processes at work. Physical models that embody known and candidate processes can be tested against observations, both in a statistical sense (possibly in the form of empirical models) and for specific events. They also integrate the available knowledge into a global perspective of the modeled system and its couplings beyond the model domain. Note that the coupling of global MHD models with inner magnetosphere models is presented in this book in Chapter 37.

22.5.1. Empirical Modeling

There are different ways to determine the plasmapause location. For instance Cho et al. (2015) used plasma density data obtained from THEMIS and looked for a density drop of a factor of 15 within a radial distance of $L = 0.5$ to estimate the plasmapause location. Subsequently, the authors developed new model fit functions for those locations in terms of the solar wind parameters and geomagnetic indices. Heilig and Lühr (2013) determined the plasmapause location from medium-scale field-aligned current observations made by CHAMP (CHAllenging Minisatellite Payload) in the topside ionosphere. After comparison with IMAGE plasmapause identifications, they derived a new empirical model of the plasmapause position in the equatorial plane.

Nikoukar et al. (2015) developed a new plasmasphere data assimilation technique using an empirical background model and GPS (Global Positioning System) data. They utilized regularization techniques by which large vertical density gradients are penalized.

Goldstein et al. (2014) used a plasmapause test particle code to simulate plasmaspheric plumes and to predict crossings at geosynchronous orbit. Their observations of fine-scale structures that appear after multiple cycles of erosion and recovery, and of the creation of successive layers of plumes, show the possibility of generating fine structure in the plasmasphere through plume merging.

For better estimating the plasmasphere contribution to the TEC for ionospheric corrections of ground-based GNSS (Global Navigation Satellite Systems) measurements, Jakowski and Hoque (2018) developed an empirical model of the plasmasphere. It utilizes electron density reconstructions from dual frequency GPS measurements on CHAMP and produces good and validated results up to $L = 3$.

Electric field models are very important for plasmaspheric studies. For example, Ridley et al. (2014) showed that the DGCPM (Dynamic Global Core Plasma Model) used during storm periods produced better results if it is driven by the Weimer (1996) model than by four other models. Therefore, it is important to improve plasmaspheric electric field models. Using Cluster data, Matsui

et al. (2013) revised their empirical model, UNH–IMEF (University of New Hampshire–Inner-Magnetospheric Electric Field), by including more data during high geomagnetic activity periods. The electric potential values are now expressed as functions of either the IEF or the *Kp* index.

Modeling plasmaspheric waves is also very useful to provide the radiation belt particle diffusion coefficients that are used in quasi-linear diffusion calculations. Accurate empirical models of wave occurrence might improve the radiation belt particle diffusion rates and lifetimes. For instance, Spasojevic et al. (2015) developed two empirical models of the average hiss wave magnetic field intensity from Van Allen Probes data.

22.5.2. Physical Modeling

A new model called NSW–GDP (New Solar Wind-driven–Global Dynamic Plasmapause) has been built based on a huge plasmapause database (49,119 crossing locations from 18 satellites during 1977–2015). This model, parameterized by solar wind parameters and geomagnetic indices, can be used for inner magnetospheric research and space weather forecasts (He et al., 2017).

A new dynamic fluid–kinetic model of the plasmasphere has been developed for investigating the plasma transport along a closed magnetic flux tube (Wang et al., 2015). By studying the behavior of heavier ions during refilling, they showed that most of O^+ ions are bouncing back and forth above the ionosphere and below the equator and then accumulate at lower altitudes.

Coupling multiple models, each describing part of the magnetospheric system, is gaining attention. For example, the coupled global ionosphere and inner magnetosphere model SAMI3/RCM has been used to describe the connection of SED (storm-time enhanced density) with plasmaspheric plumes (Huba and Sazykin, 2014).

22.5.3. Recent Modeling with Neural Networks

More recently, there have been new developments in plasmasphere modeling with the advent of neural networks.

Chu et al. (2017a) developed a neural network model of the plasmasphere electron density using density observations from equatorial satellites as the model target (output) and time series of geomagnetic and solar indices as input parameters. The architecture of the neural network is similar to that of Bortnik et al. (2016), with additional input parameters to include the contribution from ionospheric and tail processes and longer time series of indices to model more complex density features. Chu et al. (2017b) improved/expanded the model by including density observations from polar-orbiting satellites and then adding neurons in the first hidden layer (60 instead of 20, with still 10 in the second hidden layer). This new model called DEN3D (Three-Dimensional Dynamic Electron Density) successfully reproduces various well-known dynamic features in three dimensions.

Another neural network plasmaspheric density model has been developed using Van Allen Probes data for training and validation (Zhelavskaya et al., 2016). It is a feed-forward model and is called NURD (Neural-network-based Upper hybrid Resonance Determination) with one hidden layer (with 80 neurons). Using the density database obtained using NURD, they developed a new empirical model for reconstructing the global dynamics of the cold plasma density distribution in the plasmasphere, the PINE (Plasma density in the Inner magnetosphere Neural network-based Empirical) model (Zhelavskaya et al., 2017) (Figure 22.5).

22.6. THE FUTURE OF PLASMASPHERE RESEARCH

We have tried in this chapter to present most of the significant contributions to the knowledge of the plasmasphere since September 2013. However, the plasmasphere is far from being understood. Some of the remaining questions are presented in this section. We also discuss national space agency roadmaps and future mission plans. Note that the future of magnetospheric research is also treated in this book in Chapter 47.

22.6.1. Big Unsolved Questions

There is an important topic still not solved: To fully understand the circulation of dense cold plasma throughout the magnetosphere. Where does the plasmaspheric plasma go? How much exits into the magnetosheath through magnetopause reconnection and is lost to the solar wind? How much is entrained on reconnected field lines only to be drawn into the magnetotail? Can this plasma become accelerated and part of the plasmasheet to later enter pathways for energetic plasma in the magnetosphere? How much is circulated along the magnetospheric flanks into the magnetotail? How much recirculated plasmaspheric plasma returns to the ionosphere?

As discussed by Gallagher and Comfort (2016), there are many unsolved problems in plasmasphere refilling. For instance, where and when does the thermosphere influence refilling? How do the physical processes operating during refilling change in significance as refilling progresses? What is the role of ion mass and how does that role change during refilling? Do plasmas with different origins and properties, and the various processes involved, confuse our picture of plasmaspheric refilling? What is the importance of the plasmaspheric wind?

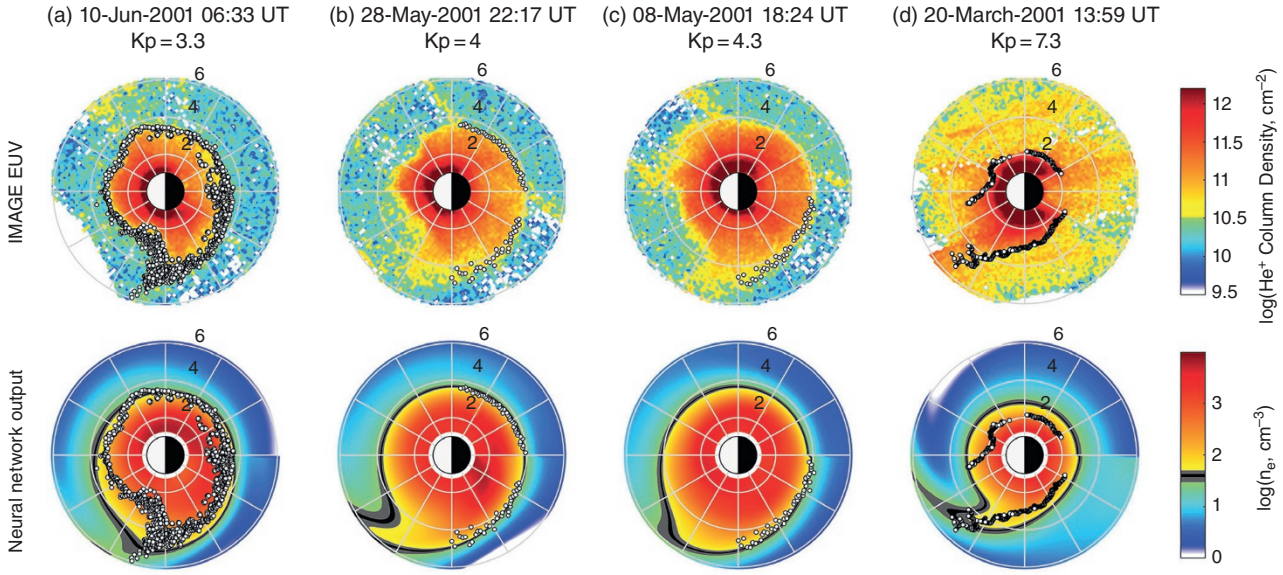

Figure 22.5 Examples of global density reconstruction by the resulting neural network model for four different events during the main phase plume formation. Top row: the EUV images for the times indicated in the titles and (bottom row) the final model output for those times. Events are ordered from left to right according to *Kp* (from low to high). *Kp* is shown in the titles as well. The Sun is to the left. (Adapted from Zhelavskaya et al., 2017.)

The importance of the interchange mechanism in plasmapause formation has been recently brought out again, through recent observations and also proposals for future NASA missions (for instance, the project TREO, Tomographic Refilling and Erosion Observatory). Are the small-scale structures formed in the plasmasphere related to this mechanism? What role does interchange play in the erosion of the plasmasphere?

Unsolved questions and problems in the magnetosphere are also presented in another chapter of this book in Chapter 46, for instance about refilling of the plasmasphere, cold plasma effects on the reconnection rate, and wave-particle interactions.

22.6.2. ESA Roadmap and US Decadal Survey

Despite the need for magnetospheric missions, and in particular inner magnetospheric missions (the last extension of the Cluster mission will end in 2022), there are at present no European Space Agency (ESA) mission plans dedicated to the Earth's inner magnetosphere. SMILE (Solar wind Magnetosphere Ionosphere Link Explorer) is a joint mission between the ESA and the Chinese Academy of Sciences (CAS) for launch in 2024. SMILE aims to build a more complete understanding of the Sun–Earth connection by measuring the solar wind and its dynamic interaction with the magnetosphere, but it does not address the inner magnetosphere. There is a candidate mission in ESA's Earth Observation program, called Daedalus, that aims to study the ionosphere and lower thermosphere, and which (if selected) could contribute knowledge regarding the origin of the ionospheric upflows that refill the plasmasphere.

In August 2012, the National Research Council of the US National Academies issued their second-ever decadal survey for solar and space physics covering the period 2013–2022 (National Research Council, 2013). One of the goals and priorities is to understand how the inner magnetosphere and plasmasphere interact with the mid-latitude ionosphere and drive its variability. One possible mission to achieve those objectives is the MEDICI (Magnetosphere Energetics, Dynamics, and Ionospheric Coupling Investigation) mission concept that aims to determine how the complex magnetosphere–ionosphere–thermosphere system is coupled and responds to external solar and internal magnetospheric forcing.

22.6.3. Recent Analysis and Future Missions

There is growing interest to renew the investigation of plasmaspheric ion composition and its dynamics using instrumentation specifically focused on this low-energy population and preventing the spacecraft floating potential from obscuring its measurement. The recent release of Dynamic Explorer 1 (DE 1) Retarding Ion Mass Spectrometer (RIMS) moments for five ion densities and temperatures is a reminder that much is yet to be learned about the plasmasphere and its relationship to ionospheric processes. Among these data the He^{++} temperatures are interestingly odd. Figure 22.6 shows He^{++} temperatures

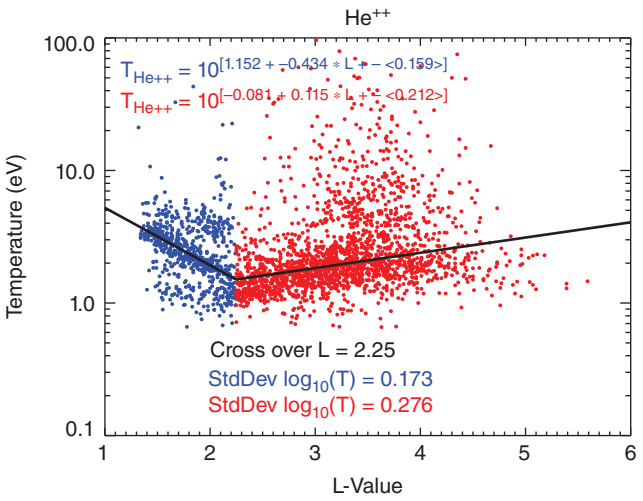

Figure 22.6 DE 1/RIMS He^{++} temperatures scatter plotted versus L values. The fit functions and standard deviations of the fit parameters are also shown in the figure. The data set is available from: https://plasmasphere.nasa.gov/rims/.

scatter plotted versus L values. Temperatures are found to initially fall with increasing L value before rising after $L = 2.25$. There is the suggestion that the low and high L value populations overlap slightly, hence may reveal distinct populations. The solid lines are linear fits to the logarithm based 10 of temperature. These data suggest the presence of another population at twice the He^{++} temperature at low L values. In fact, the RIMS and moments analysis is consistent with this populations being Deuterium ions. The fit functions and standard deviations of the fit parameters are also shown in the figure.

Several teams of researchers are independently pursuing the design and support for resuming the investigation of cold plasmaspheric plasma. Mission concepts may be expected to include new in situ measurements of composition with a design emphasis on low energies, rather than recent attempts to do all with one instrument across a wide range of energies. Spacecraft charging is recognized as presenting a continuing challenge for measuring ions below a few eV in energy that must be overcome before the characterization of this population can be advanced. Full phase-space ion distributions are also known to be important for quantifying field-aligned versus cross-field transport. Plasmasphere refilling from the ionosphere remains poorly understood. It has only recently been recognized that earlier, presumed measurements of heated plasmaspheric plasma may have included the lower energy portion of the warm plasma cloak that have arrived in the nightside inner magnetosphere by convection from high-latitude cleft fountain and auroral outflow. The ground breaking He^{+} imaging by the IMAGE EUV instrument may be followed by O^{+} imaging as studied by Goldstein et al. (2018). They studied the possibilities of building a 83.4 nm oxygen imager and developed a viable technique to understand better outflow and refilling and the dynamical influence of regions of enhanced oxygen density. And last, but not least, the use of more than one spacecraft might enable continuous monitoring of plasmasphere dynamics and stereo or better imaging to obtain 3-D plasma distributions.

ACKNOWLEDGMENTS

F. Darrouzet and J. De Keyser thank the ESA for the Cluster mission and the Cluster Science Archive (CSA, http://www.cosmos.esa.int/web/csa/access) for access to orbital parameters. F. Darrouzet and J. De Keyser acknowledge BIRA-IASB (Royal Belgian Institute for Space Aeronomy), STCE (Solar-Terrestrial Center of Excellence) and BELSPO (Belgian Federal Science Policy Office) for their support through a Prodex project (contract 13127/98/NL/VJ).

REFERENCES

Adrian, M. L., S. F. Fung, D. L. Gallagher, and J. L. Green (2015), Whistlers observed outside the plasmasphere: Correlation to plasmaspheric/plasmapause features, *Journal of Geophysical Research: Space Physics*, 120(9), 7585–7614, doi:10.1002/2014JA020811.

André, M., K. Li, and A. I. Eriksson (2015), Outflow of low-energy ions and the solar cycle, *Journal of Geophysical Research: Space Physics*, 120(2), 1072–1085, doi:10.1002/2014JA020714.

Bandić, M., G. Verbanac, M. B. Moldwin, V. Pierrard, and G. Piredda (2016), MLT dependence in the relationship between plasmapause, solar wind, and geomagnetic activity based on CRRES: 1990-1991, *Journal of Geophysical Research: Space Physics*, 121(5), 4397–4408, doi:10.1002/2015JA022278.

Boardsen, S. A., M. L. Adrian, R. Pfaff, and J. D. Menietti (2014), Inner magnetospheric electron temperature and spacecraft potential estimated from concurrent Polar upper hybrid frequency and relative potential measurements, *Journal of Geophysical Research: Space Physics*, 119(10), 8046–8062, doi:10.1002/2014JA019852.

Borovsky, J. E., R. H.W. Friedel, and M. H. Denton (2014), Statistically measuring the amount of pitch angle scattering that energetic electrons undergo as they drift across the plasmaspheric drainage plume at geosynchronous orbit, *Journal of Geophysical Research: Space Physics*, 119(3), 1814–1826, doi:10.1002/2013JA019310.

Bortnik, J., W. Li, R. M. Thorne, and V. Angelopoulos (2016), A unified approach to inner magnetospheric state prediction, *Journal of Geophysical Research: Space Physics*, 121(3), 2423–2430, doi:10.1002/2015JA021733.

Brito, T., M. K. Hudson, B. Kress, J. Paral, A. Halford, R. Millan, and M. Usanova (2015), Simulation of ULF wave-modulated radiation belt electron precipitation during the

17 March 2013 storm, *Journal of Geophysical Research: Space Physics*, 120(5), 3444–3461, doi:10.1002/2014JA020838.

Chen, C. Y., T. J. Y. Liu, I. T. Lee, H. Rothkaehl, D. Przepiorka, L. C. Chang, et al. (2018), The midlatitude trough and the plasmapause in the nighttime ionosphere simultaneously observed by DEMETER during 2006-2009, *Journal of Geophysical Research: Space Physics*, 123(7), 5917–5932, doi:10.1029/2017JA024840.

Chi, P. J., M. J. Engebretson, M. B. Moldwin, C. T. Russell, I. R. Mann, M. R. Hairston, et al. (2013), Sounding of the plasmasphere by Mid-continent MAgnetoseismic Chain (McMAC) magnetometers, *Journal of Geophysical Research: Space Physics*, 118(6), 3077–3086, doi:10.1002/jgra.50274.

Cho, J., D.-Y. Lee, J.-H. Kim, D.-K. Shin, K.-C. Kim, and D. Turner (2015), New model fit functions of the plasmapause location determined using THEMIS observations during the ascending phase of Solar Cycle 24, *Journal of Geophysical Research: Space Physics*, 120(4), 2877–2889, doi:10.1002/2015JA021030.

Chu, X., J. Bortnik, W. Li, Q. Ma, V. Angelopoulos, and R. M. Thorne (2017a), Erosion and refilling of the plasmasphere during a geomagnetic storm modeled by a neural network, *Journal of Geophysical Research: Space Physics*, 122(7), 7118–7129, doi:10.1002/2017JA023948.

Chu, X., J. Bortnik, W. Li, Q. Ma, R. Denton, C. Yue, et al. (2017b), A neural network model of three-dimensional dynamic electron density in the inner magnetosphere, *Journal of Geophysical Research: Space Physics*, 122(9), 9183–9197, doi:10.1002/2017JA024464.

Chugunin, D. V., G. A. Kotova, M. V. Klimenko, and V. V. Klimenko (2017), Longitudinal dependence of the H+ concentration distribution in the plasmasphere according to Interball-1 satellite data, *Cosmic Research*, 55(6), 457–463, doi:10.1134/S001095251706003X.

Dandouras, I. (2013), Detection of a plasmaspheric wind in the Earth's magnetosphere by the Cluster spacecraft, *Annales Geophysicae*, 31(7), 1143–1153, doi:10.5194/angeo-31-1143-2013.

Darrouzet, F., and J. De Keyser (2013), The dynamics of the plasmasphere: Recent results, *Journal of Atmospheric and Solar-Terrestrial Physics*, 99(7), 53–60, doi:10.1016/j.jastp.2012.07.004.

Darrouzet, F., J. De Keyser, and V. Pierrard (Eds.) (2009), *The Earth's plasmasphere: A cluster and image perspective*. Springer, New York, doi:10.1007/978-1-4419-1323-4.

Darrouzet, F., V. Pierrard, S. Benck, G. Lointier, J. Cabrera, K. Borremans, et al. (2013), Links between the plasmapause and the radiation belt boundaries as observed by the instruments CIS, RAPID, and WHISPER onboard Cluster, *Journal of Geophysical Research: Space Physics*, 118(7), 4176–4188, doi:10.1002/jgra.50239.

Décréau, P. M. E., S. Kougblénou, G. Lointier, J.-L. Rauch, J.-G. Trotignon, X. Vallières, et al. (2013), Remote sensing of a NTC radio source from a Cluster tilted spacecraft pair, *Annales Geophysicae*, 31(11), 2097–2121, doi:10.5194/angeo-31-2097-2013.

Décréau, P. M. E., S. Aoutou, A. Denazelle, I. Galkina, J.-L. Rauch, X. Vallières, et al. (2015), Widebanded NTC radiation: local to remote observations by the four Cluster satellites, *Annales Geophysicae*, 33(10), 1285–1300, doi:10.5194/angeo-33-1285-2015.

Denton, M. H., and J. E. Borovsky (2014), Observations and modeling of magnetic flux tube refilling of the plasmasphere at geosynchronous orbit, *Journal of Geophysical Research: Space Physics*, 119(11), 9246–9255, doi:10.1002/2014JA020491.

Denton, R. E., K. Takahashi, M. F. Thomsen, J. E. Borovsky, H. J. Singer, Y. Wang, et al. (2014), Evolution of mass density and O+ concentration at geostationary orbit during storm and quiet events, *Journal of Geophysical Research: Space Physics*, 119(8), 6417–6431, doi:10.1002/2014JA019888.

Erickson, P. J., H. Matsui, J. C. Foster, R. B. Torbert, R. E. Ergun, Y. V. Khotyaintsev, et al. (2016), Multipoint MMS observations of fine-scale SAPS structure in the inner magnetosphere, *Geophysical Research Letters*, 43(14), 7294–7300, doi:10.1002/2016GL069174.

Foster, J. C., P. J. Erickson, A. J. Coster, S. Thaller, J. Tao, J. R. Wygant, and J. W. Bonnell (2014), Storm time observations of plasmasphere erosion flux in the magnetosphere and ionosphere, *Geophysical Research Letters*, 41(3), 762–768, doi:10.1002/2013GL059124.

Fuselier, S. A., J. L. Burch, P. A. Cassak, J. Goldstein, R. G. Gomez, K. Goodrich, et al. (2016), Magnetospheric ion influence on magnetic reconnection at the duskside magnetopause, *Geophysical Research Letters*, 43(4), 1435–1442, doi:10.1002/2015GL067358.

Gallagher, D. L., and R. H. Comfort (2016), Unsolved problems in plasmasphere refilling, *Journal of Geophysical Research: Space Physics*, 121(2), 1447–1451, doi:10.1002/2015JA022279.

Genestreti, K. J., J. Goldstein, G. D. Corley, W. Farner, L. M. Kistler, B. A. Larsen, et al. (2017), Temperature of the plasmasphere from Van Allen Probes HOPE, *Journal of Geophysical Research: Space Physics*, 122(1), 310–323, doi:10.1002/2016JA023047.

Goldstein, J., M. F. Thomsen, and A. DeJong (2014), In situ signatures of residual plasmaspheric plumes: Observations and simulation, *Journal of Geophysical Research: Space Physics*, 119(6), 4706–4722, doi:10.1002/2014JA019953.

Goldstein, J., D. N. Baker, J. B. Blake, S. De Pascuale, H. O. Funsten, A. N. Jaynes, et al. (2016), The relationship between the plasmapause and outer belt electrons, *Journal of Geophysical Research: Space Physics*, 121(9), 8392–8416, doi:10.1002/2016JA023046.

Goldstein, J., D. Gell, and B. R. Sandel (2017), Empirical determination of extreme ultraviolet imager background, *Journal of Geophysical Research: Space Physics*, 122(7), 7414–7432, doi:10.1002/2017JA024301.

Goldstein, J., C. R. Chappell, M. W. Davis, M. H. Denton, R. E. Denton, D. L. Gallagher, et al. (2018), Imaging the global distribution of plasmaspheric oxygen, *Journal of Geophysical Research: Space Physics*, 123(3), 2078–2103, doi:10.1002/2017JA024531.

Green, J. L. (2015), IMAGE Mission: Imager for magnetopause-to-aurora global exploration. In J. N. Pelton and F. Allahdadi (Eds.), *Handbook of cosmic hazards and planetary defense* (pp. 345–358). Springer International Publishing, doi:10.1007/978-3-319-03952-7-29.

Grison, B., F. Darrouzet, O. Santolík, N. Cornilleau-Wehrlin, and A. Masson (2016), Cluster observations of reflected EMIC-triggered emission, *Geophysical Research Letters*, 43 (9), 4164–4171, doi:10.1002/2016GL069096.

Grison, B., M. Hanzelka, H. Breuillard, F. Darrouzet, O. Santolík, N. Cornilleau-Wehrlin, and I. Dandouras (2018), Plasmaspheric plumes and EMIC rising tone emissions, *Journal of Geophysical Research: Space Physics*, 123(11), 9443–9452, doi:10.1029/2018JA025796.

Halford, A. J., B. J. Fraser, and S. K. Morley (2015), EMIC waves and plasmaspheric and plume density: CRRES results, *Journal of Geophysical Research: Space Physics*, 120(3), 1974–1992, doi:10.1002/2014JA020338.

Hartley, D. P., C. A. Kletzing, S. De Pascuale, W. S. Kurth, and O. Santolík (2018), Determining plasmaspheric densities from observations of plasmaspheric hiss, *Journal of Geophysical Research: Space Physics*, 123(8), 6679–6691, doi:10.1029/2018JA025658.

He, F., X.-X. Zhang, B. Chen, M.-C. Fok, and S. Nakano (2016), Determination of the Earth's plasmapause location from the CE-3 EUVC images, *Journal of Geophysical Research: Space Physics*, 121(1), 296–304, doi:10.1002/2015JA021863.

He, F., X.-X. Zhang, R.-L. Lin, M.-C. Fok, R. M. Katus, M. W. Liemohn, et al. (2017), A new solar wind-driven global dynamic plasmapause model: 2. Model and validation, *Journal of Geophysical Research: Space Physics*, 122(7), 7172–7187, doi:10.1002/2017JA023913.

Heilig, B., and H. Lühr (2013), New plasmapause model derived from CHAMP field-aligned current signatures, *Annales Geophysicae*, 31(3), 529–539, doi:10.5194/angeo-31-529-2013.

Heilig, B., and H. Lühr (2018), Quantifying the relationship between the plasmapause and the inner boundary of small-scale field-aligned currents, as deduced from Swarm observations, *Annales Geophysicae*, 36(2), 595–607, doi:10.5194/angeo-36-595-2018.

Huba, J. D., and S. Sazykin (2014), Storm time ionosphere and plasmasphere structuring: SAMI3-RCM simulation of the 31 March 2001 geomagnetic storm, *Geophysical Research Letters*, 41(23), 8208–8214, doi:10.1002/2014GL062110.

Hudson, M. K., D. N. Baker, J. Goldstein, B. T. Kress, J. Paral, F. R. Toffoletto, and M. Wiltberger (2014), Simulated magnetopause losses and Van Allen Probe flux dropouts, *Geophysical Research Letters*, 41(4), 1113–1118, doi:10.1002/2014GL059222.

Jakowski, N., and M. M. Hoque (2018), A new electron density model of the plasmasphere for operational applications and services, *Journal of Space Weather and Space Climate*, 8, A16, doi:10.1051/swsc/2018002.

Katus, R. M., D. L. Gallagher, M. W. Liemohn, A. M. Keesee, and L. K. Sarno-Smith (2015), Statistical storm time examination of MLT-dependent plasmapause location derived from IMAGE EUV, *Journal of Geophysical Research: Space Physics*, 120(7), 5545–5559, doi:10.1002/2015JA021225.

Kotova, G., M. Verigin, and V. Bezrukikh (2014), The effect of the Earth's optical shadow on thermal plasma measurements in the plasmasphere, *Journal of Atmospheric and Solar-Terrestrial Physics*, 120, 9–14, doi:10.1016/j.jastp.2014.08.013.

Kotova, G., M. Verigin, J. Lemaire, V. Pierrard, V. Bezrukikh, and J. Smilauer (2018), Experimental study of the plasmasphere boundary layer using MAGION 5 data, *Journal of Geophysical Research: Space Physics*, 123(2), 1251–1259, doi:10.1002/2017JA024590.

Krall, J., J. T. Emmert, F. Sassi, S. E. McDonald, and J. D. Huba (2016), Day-to-day variability in the thermosphere and its impact on plasmasphere refilling, *Journal of Geophysical Research: Space Physics*, 121(7), 6889–6900, doi:10.1002/2015JA022328.

Krall, J., J. D. Huba, and S. Sazykin (2017), Erosion of the plasmasphere during a storm, *Journal of Geophysical Research: Space Physics*, 122(9), 9320–9328, doi:10.1002/2017JA024450.

Kwon, H.-J., K.-H. Kim, G. Jee, J.-S. Park, H. Jin, and Y. Nishimura (2015), Plasmapause location under quiet geomagnetic conditions ($Kp \leq 1$): THEMIS observations, *Geophysical Research Letters*, 42(18), 7303–7310, doi:10.1002/2015GL066090.

Laakso, H., O. Santolík, R. Horne, I. Kolmašová, P. Escoubet, A. Masson, and M. Taylor (2015), Identifying the source region of plasmaspheric hiss, *Geophysical Research Letters*, 42(9), 3141–3149, doi:10.1002/2015GL063755.

Lee, H.-B., G. Jee, Y. H. Kim, and J. S. Shim (2013), Characteristics of global plasmaspheric TEC in comparison with the ionosphere simultaneously observed by Jason-1 satellite, *Journal of Geophysical Research: Space Physics*, 118(2), 935–946, doi:10.1002/jgra.50130.

Lee, S. H., H. Zhang, Q.-G. Zong, A. Otto, H. Rme, and E. Liebert (2016), A statistical study of plasmaspheric plumes and ionospheric outflows observed at the dayside magnetopause, *Journal of Geophysical Research: Space Physics*, 121(1), 492–506, doi:10.1002/2015JA021540.

Lemaire, J. F., and K. I. Gringauz (1998), *The Earth's plasmasphere*, Cambridge University Press, New York.

Li, W., R. M. Thorne, J. Bortnik, G. D. Reeves, C. A. Kletzing, W. S. Kurth, et al. (2013), An unusual enhancement of low-frequency plasmaspheric hiss in the outer plasmasphere associated with substorm-injected electrons, *Geophysical Research Letters*, 40(15), 3798–3803, doi:10.1002/grl.50787.

Liu, W., J. B. Cao, X. Li, T. E. Sarris, Q.-G. Zong, M. Hartinger, et al. (2013), Poloidal ULF wave observed in the plasmasphere boundary layer, *Journal of Geophysical Research: Space Physics*, 118(7), 4298–4307, doi:10.1002/jgra.50427.

Loi, S. T., T. Murphy, I. H. Cairns, F. W. Menk, C. L. Waters, P. J. Erickson, et al. (2015), Real-time imaging of density ducts between the plasmasphere and ionosphere, *Geophysical Research Letters*, 42(10), 3707–3714, doi:10.1002/2015GL063699.

Lointier, G., F. Darrouzet, P. M. E. Décréau, X. Vallières, S. Kougblénou, J.-G. Trotignon, and J.-L. Rauch (2013), Refilling process in the plasmasphere: a 3-D statistical characterization based on Cluster density observations, *Annales Geophysicae*, 31(2), 217–237, doi:10.5194/angeo-31-217-2013.

Ma, Q., D. Mourenas, W. Li, A. Artemyev, and R. M. Thorne (2017), VLF waves from ground-based transmitters observed by the Van Allen Probes: Statistical model and effects on plasmaspheric electrons, *Geophysical Research Letters*, 44(13), 6483–6491, doi:10.1002/2017GL073885.

Malaspina, D. M., J.-F. Ripoll, X. Chu, G. Hospodarsky, and J. Wygant (2018), Variation in plasmaspheric hiss wave power with plasma density, *Geophysical Research Letters*, 45(18), 9417–9426, doi:10.1029/2018GL078564.

Matsui, H., R. B. Torbert, H. E. Spence, Y. V. Khotyaintsev, and P.-A. Lindqvist (2013), Revision of empirical electric field modeling in the inner magnetosphere using luster data, *Journal of Geophysical Research: Space Physics*, 118(7), 4119–4134, doi:10.1002/jgra.50373.

Menk, F., Z. Kale, M. Sciffer, P. Robinson, C. Waters, R. Grew, et al. (2014), Remote sensing the plasmasphere, plasmapause, plumes and other features using ground-based magnetometers, *Journal of Space Weather and Space Climate*, 4, A34, doi:10.1051/swsc/2014030.

Meredith, N. P., R. B. Horne, T. Kersten, W. Li, J. Bortnik, A. Sicard, and K. H. Yearby (2018), Global model of plasmaspheric hiss from multiple satellite observations, *Journal of Geophysical Research: Space Physics*, 123(6), 4526–4541, doi:10.1029/2018JA025226.

Moldwin, M. B., S. Zou, and T. Heine (2016), The story of plumes: the development of a new conceptual framework for understanding magnetosphere and ionosphere coupling, *Annales Geophysicae*, 34(12), 1243–1253, doi:10.5194/angeo-34-1243-2016.

Nakano, S., M.-C. Fok, P. C. Brandt, and T. Higuchi (2014), Estimation of temporal evolution of the helium plasmasphere based on a sequence of IMAGE/EUV images, *Journal of Geophysical Research: Space Physics*, 119(5), 3708–3723, doi:10.1002/2013JA019734.

National Research Council (2013), *Solar and space physics: A science for a technological society*, The National Academies Press, Washington, DC, doi:10.17226/13060.

Nikoukar, R., G. Bust, and D. Murr (2015), A novel data assimilation technique for the plasmasphere, *Journal of Geophysical Research: Space Physics*, 120(10), 8470–8485, doi:10.1002/2015JA021455.

Ouellette, J. E., J. G. Lyon, O. J. Brambles, B. Zhang, and W. Lotko (2016), The effects of plasmaspheric plumes on dayside reconnection, *Journal of Geophysical Research: Space Physics*, 121(5), 4111–4118, doi:10.1002/2016JA022597.

Reddy, A., V. S. Sonwalkar, and J. D. Huba (2018), Evolution of field-aligned electron and ion densities from whistler mode radio soundings during quiet to moderately active period and comparisons with SAMI2 simulations, *Journal of Geophysical Research: Space Physics*, 123(2), 1356–1380, doi:10.1002/2017JA024348.

Ren, J., Q. G. Zong, Y. Miyoshi, R. Rankin, H. E. Spence, H. O. Funsten, J. R. Wygant, and C. A. Kletzing (2018), A comparative study of ULF waves' role in the dynamics of charged particles in the plasmasphere: Van Allen Probes observation, *Journal of Geophysical Research: Space Physics*, 123(7), 5334–5343, doi:10.1029/2018JA025255.

Ridley, A., A. M. Dodger, and M. W. Liemohn (2014), Exploring the efficacy of different electric field models in driving a model of the plasmasphere, *Journal of Geophysical Research: Space Physics*, 119(6), 4621–4638, doi:10.1002/2014JA019836.

Santolík, O., M. Parrot, and F. Němec (2016), Propagation of equatorial noise to low altitudes: Decoupling from the magnetosonic mode, *Geophysical Research Letters*, 43(13), 6694–6704, doi:10.1002/2016GL069582.

Sarno-Smith, L. K., M. W. Liemohn, R. M. Katus, R. M. Skoug, B. A. Larsen, M. F. Thomsen, et al. (2015), Postmidnight depletion of the high-energy tail of the quiet plasmasphere, *Journal of Geophysical Research: Space Physics*, 120(3), 1646–1660, doi:10.1002/2014JA020682.

Shim, J. S., G. Jee, and L. Scherliess (2017), Climatology of plasmaspheric total electron content obtained from Jason 1 satellite, *Journal of Geophysical Research: Space Physics*, 122(2), 1611–1623, doi:10.1002/2016JA023444.

Spasojevic, M., Y. Y. Shprits, and K. Orlova (2015), Global empirical models of plasmaspheric hiss using Van Allen Probes, *Journal of Geophysical Research: Space Physics*, 120(12), 10370–10383, doi:10.1002/2015JA021803.

Su, Z., N. Liu, H. Zheng, Y. Wang, and S. Wang (2018), Large-amplitude extremely low frequency hiss waves in plasmaspheric plumes, *Geophysical Research Letters*, 45(2), 565–577, doi:10.1002/2017GL076754.

Summers, D., Y. Omura, S. Nakamura, and C. A. Kletzing (2014), Fine structure of plasmaspheric hiss, *Journal of Geophysical Research: Space Physics*, 119(11), 9134–9149, doi:10.1002/2014JA020437.

Toledo-Redondo, S., M. Andr, A. Vaivads, Y. V. Khotyaintsev, B. Lavraud, D. B. Graham, et al. (2016), Cold ion heating at the dayside magnetopause during magnetic reconnection, *Geophysical Research Letters*, 43(1), 58–66, doi:10.1002/2015GL067187.

Turner, D. L., S. G. Claudepierre, J. F. Fennell, T. P. O'Brien, J. B. Blake, C. Lemon, et al. (2015), Energetic electron injections deep into the inner magnetosphere associated with substorm activity, *Geophysical Research Letters*, 42(7), 2079–2087, doi:10.1002/2015GL063225.

Usanova, M. E., and Y. Y. Shprits (2017), Inner magnetosphere coupling: Recent advances, *Journal of Geophysical Research: Space Physics*, 122(1), 102–104, doi:10.1002/2016JA023614.

Usanova, M. E., F. Darrouzet, I. R. Mann, and J. Bortnik (2013), Statistical analysis of EMIC waves in plasmaspheric plumes from Cluster observations, *Journal of Geophysical Research: Space Physics*, 118(8), 4946–4951, doi:10.1002/jgra.50464.

Usanova, M. E., I. R. Mann, and F. Darrouzet (2016), EMIC Waves in the inner magnetosphere. In A. Keiling, D.-H. Lee, and V. Nakariakov (Eds.), *Low-frequency waves in space plasmas, Geophysical Monograph Series* (Vol. 216, pp. 65–78). American Geophysical Union (AGU), doi:10.1002/9781119055006.ch5.

Verbanac, G., V. Pierrard, M. Bandić, F. Darrouzet, J.-L. Rauch, and P. Décréau (2015), The relationship between plasmapause, solar wind and geomagnetic activity between 2007 and 2011, *Annales Geophysicae*, 33(10), 1271–1283, doi:10.5194/angeo-33-1271-2015.

Walsh, B. M., D. G. Sibeck, Y. Nishimura, and V. Angelopoulos (2013), Statistical analysis of the plasmaspheric plume at the magnetopause, *Journal of Geophysical Research: Space Physics*, 118(8), 4844–4851, doi:10.1002/jgra.50458.

Walsh, B. M., J. C. Foster, P. J. Erickson, and D. G. Sibeck (2014), Simultaneous ground- and space-based observations

of the plasmaspheric plume and reconnection, *Science*, 343 (6175), 1122–1125, doi:10.1126/science.1247212.

Wang, Y., J. Tu, and P. Song (2015), A new dynamic fluid-kinetic model for plasma transport within the plasmasphere, *Journal of Geophysical Research: Space Physics*, 120(10), 8486–8502, doi:10.1002/2015JA021345.

Wang, Y., J. Tu, and P. Song (2016), Mass loading at the magnetopause through the plasmaspheric plume, *Journal of Geophysical Research: Space Physics*, 121(10), 9501–9516, doi:10.1002/2016JA022395.

Weimer, D. R. (1996), A flexible, IMF dependent model of high-latitude electric potentials having Space Weather applications, *Geophysical Research Letters*, 23(18), 2549–2552, doi:10.1029/96GL02255.

Whittaker, I. C., M. A. Clilverd, and C. J. Rodger (2014), Characteristics of precipitating energetic electron fluxes relative to the plasmapause during geomagnetic storms, *Journal of Geophysical Research: Space Physics*, 119(11), 8784–8800, doi:10.1002/2014JA020446.

Woodroffe, J. R., V. K. Jordanova, H. O. Funsten, A. V. Streltsov, M. T. Bengtson, C. A. Kletzing, et al. (2017), Van Allen Probes observations of structured whistler mode activity and coincident electron Landau acceleration inside a remnant plasmaspheric plume, *Journal of Geophysical Research: Space Physics*, 122(3), 3073–3086, doi:10.1002/2015JA022219.

Xiao, F., Q. Zhou, Y. He, C. Yang, S. Liu, D. N. Baker, et al. (2015), Penetration of magnetosonic waves into the plasmasphere observed by the Van Allen Probes, *Geophysical Research Letters*, 42(18), 7287–7294, doi:10.1002/2015GL065745.

Yahnin, A. G., T. Yahnina, H. Frey, and V. Pierrard (2013), Sub-oval proton aurora spots: Mapping relatively to the plasmapause, *Journal of Atmospheric and Solar-Terrestrial Physics*, 99, 61–66, doi:10.1016/j.jastp.2012.09.018.

Yan, Y., H.-N. Wang, H. He, F. He, B. Chen, J.-Q. Feng, et al. (2016), Analysis of observational data from Extreme Ultra-Violet Camera onboard Chang'e-3 mission, *Astrophysics and Space Science*, 361(2), 76, doi:10.1007/s10509-016-2650-2.

Yu, J., L. Y. Li, J. Cui, and J. Wang (2018), Ultrawideband risingtone chorus waves observed inside the oscillating plasmapause, *Journal of Geophysical Research: Space Physics*, 123(8), 6670–6678, doi:10.1029/2018JA025875.

Yuan, Z., Y. Xiong, S. Huang, X. Deng, Y. Pang, M. Zhou, et al. (2014), Cold electron heating by EMIC waves in the plasmaspheric plume with observations of the Cluster satellite, *Geophysical Research Letters*, 41(6), 1830–1837, doi:10.1002/2014GL059241.

Yue, C., J. Bortnik, W. Li, Q. Ma, M. Gkioulidou, G. D. Reeves, et al. (2018), The composition of plasma inside geostationary orbit based on Van Allen Probes observations, *Journal of Geophysical Research: Space Physics*, 123(8), 6478–6493, doi:10.1029/2018JA025344.

Zhang, Q., M. Lockwood, J. C. Foster, Q. Zong, M. W. Dunlop, S. Zhang, et al. (2018a), Observations of the step-like accelerating processes of cold ions in the reconnection layer at the dayside magnetopause, *Science Bulletin*, 63(1), 31–37, doi:10.1016/j.scib.2018.01.003.

Zhang, W., S. Fu, X. Gu, B. Ni, Z. Xiang, D. Summers, et al. (2018b), Electron scattering by plasmaspheric hiss in a nightside plume, *Geophysical Research Letters*, 45(10), 4618–4627, doi:10.1029/2018GL077212.

Zhang, X. X., F. He, B. Chen, C. Shen, and H. N. Wang (2017), Correlations between plasmapause evolutions and auroral signatures during substorms observed by Chang'e-3 EUV Camera, *Earth and Planetary Physics*, 1(1), 35–43, doi:10.26464/epp2017005.

Zhelavskaya, I. S., M. Spasojević, Y. Y. Shprits, and W. S. Kurth (2016), Automated determination of electron density from electric field measurements on the Van Allen Probes spacecraft, *Journal of Geophysical Research: Space Physics*, 121(5), 4611–4625, doi:10.1002/2015JA022132.

Zhelavskaya, I. S., Y. Y. Shprits, and M. Spasojević (2017), Empirical modeling of the plasmasphere dynamics using neural networks, *Journal of Geophysical Research: Space Physics*, 122(11), 11227–11244, doi:10.1002/2017JA024406.

Zong, Q.-G., Y. F. Wang, J. Ren, X. Z. Zhou, S. Y. Fu, R. Rankin, and H. Zhang (2017), Corotating drift-bounce resonance of plasmaspheric electron with poloidal ULF waves, *Earth and Planetary Physics*, 1(1), 2–12, doi:10.26464/epp2017002.